

Towards Cooperative Transport of a Suspended Payload via Two Aerial Robots with Inertial Sensing

Heng Xie, Xinyu Cai, and Pakpong Chirarattananon

Abstract—This paper addresses the problem of cooperative transport of a point mass hoisted by two aerial robots. Treating the robots as a leader and a follower, the follower stabilizes the system with respect to the leader using only feedback from its Inertial Measurement Units (IMU). This is accomplished by neglecting the acceleration of the leader, analyzing the system through the generalized coordinates or the cables' angles, and employing an observation model based on the IMU measurements. A lightweight estimator based on an Extended Kalman Filter (EKF) and a controller are derived to stabilize the robot-payload-robot system. The proposed methods are verified with extensive flight experiments, first with a single robot and then with two robots. The results show that the follower is capable of realizing the desired quasi-static trajectory using only its IMU measurements. The outcomes demonstrate promising progress towards the goal of autonomous cooperative transport of a suspended payload via small flying robots with minimal sensing and computational requirements.

I. INTRODUCTION

In the past decades, we have witnessed a rapid development of small flying robots [1], [2]. The development of miniaturized electronics and associated algorithms allows these Micro Aerial Vehicles (MAVs) to be used for surveillance, mapping, agriculture, delivery, etc. Owing to their small footprint, more recently, there has been a growing interest in the use of these small drones in collaborative tasks, including for swarm behavior [3], manipulation [4] or collective transportation of heavy objects either by rigid attachments [5]–[8] or suspension [9], [10].

This paper focuses on the cooperative transport of a suspended payload by multiple MAVs. In early stages, the problem of aerial transport of a suspended payload has been considered in the single-robot context [11]–[15]. To increase the load-carrying capacity, uses of multiple vehicles emerge as an appealing solution [6], [9]. However, the strategy inevitably results in additional complications as the dynamics of multiple robots and the payload become coupled.

As a result, studies concerning cooperative manipulation of a payload suspended from multiple robots focus on the dynamics, trajectory generation, and control [9], [10], [16]. In [9], the authors showed that the system of multiple robots carrying a point mass or rigid body payload is differentially flat when the trajectory of the payload is chosen as the flat output. The framework assists in the computation of

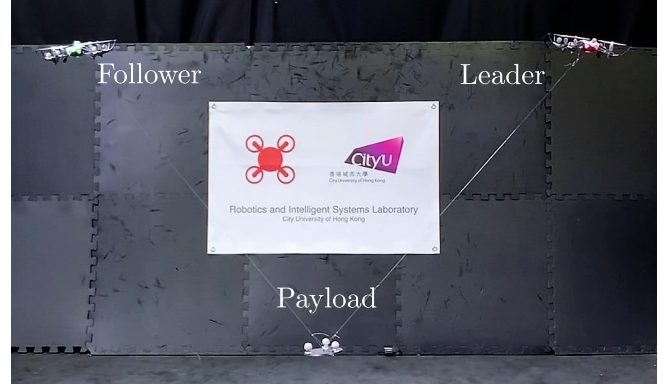


Fig. 1. Two robots in a leader-follower configuration transporting a point-mass payload. The formation is stabilized by the follower robot using only feedback from its IMU.

the trajectories of associated robots, allowing the collective transport task to be realized in actual experiments. Nevertheless, similar to other related works [16]–[18], the proposed solution necessitates comprehensive feedback of robots' pose and global communication, limiting the application to laboratory environments with a motion capture system and global communication as found in [16] or simulation as shown by [17], [18].

The feedback and communication issue has recently been tackled by incorporating vision [10] (and [6], [8] for a rigidly attached payload). The method in [10] employs a leader-follower approach. This requires two robots to visually track the transported object and the follower to directly observe the leader. Similarly, vision has been used to estimate the pose of the robot-payload-robot formation [6] or to estimate the force applied to the payload by the other robot [8]. While these approaches do not require explicit communication between agents, the deployments rely heavily on visual feedback, amplifying the computational cost and sensory payload, rendering it unsuitable for smaller flying robots.

This work offers an alternative strategy for the transportation of a point-mass payload hoisted by two robots as portrayed in Fig. 1. The proposed method requires only the IMU and no communication between two robots. The limitation to two-robot scenarios let us treat the robots as a leader and a follower. By restricting to non-aggressive maneuvers or neglecting the acceleration of the leader (this does not prevent the robots to traverse at moderate or high speed), the desired quasi-static trajectory is essentially stabilized by the follower. To achieve this, the follower robot uses only IMU feedback to estimate the state, or its relative position to the leader, via the developed EKF-based estimator. Then, a controller

This work was supported by the Research Grants Council of the Hong Kong Special Administrative Region of China (grant number CityU-11215117).

The authors are with the Department of Biomedical Engineering, City University of Hong Kong, Hong Kong SAR, China (email: pakpong.c@cityu.edu.hk).

is derived based on the linearized dynamics. To this end, the state dynamics are stabilized according to the estimated state vector computed entirely from the IMU measurements. Despite some constraints in the current implementation, this framework provides a novel approach for aerial collective transport with minimal sensing requirements.

This paper is organized as follows. In Section II, the simplified dynamics of leader-payload-follower system are given. This includes the observation model that leads to the derivation of the state estimator and controller in Section III. Flight experiments are performed in Section IV to evaluate the performance of the proposed estimator and controller. Conclusion and discussion of possible extensions of this work are given in Section V.

II. LEADER-FOLLOWER SYSTEM DYNAMICS

This work consider a transportation of single payload suspended between two aerial robots in the leader-follower manner with cables are presumed massless and always taut. To simplify the consideration, the leader's dynamics are assumed quasi-static—its acceleration is negligible. Additional aerodynamic damping forces are also neglected. Presently, this limits the operating conditions to low-to-moderate speed flights with small accelerations.

A. Reduced Dynamic Model

Fig. 2 illustrates planar views of the coordinate frames and associated parameters of the two-robot system. The origin of frame $\mathcal{P} : \{x_p, y_p, z_p\}$ is assumed coincident with the center-of-mass (CoM) of the leader. Thanks to the near-hovering assumption, frame \mathcal{P} is regarded as an inertial frame, allowing the dynamics of the leader to be neglected. Frame $\mathcal{B} : \{x_b, y_b, z_b\}$ is a body-fixed frame associated with the follower. The follower, with mass m , generates a collective thrust f in the direction opposite to z_b . The payload, with mass M , is a point mass hoisted between two robots by massless cables with lengths l_0 and l_1 . The cable's attachment point passes through the CoM of the robot. Consequently the cable tension makes no contribution to the attitude dynamics of the follower. Positions of the payload and the follower with respect to \mathcal{P} , denoted by \mathbf{r}_0 and \mathbf{r}_1 , are described by the angles of the cable ϕ_0 and ϕ_1 measured from the vertical about x_p . Since the pitch and yaw dynamics of the follower are not directly affected by the suspended payload, at this stage, they are assumed to be separately controlled such that the yaw angle is always zero (hence, y_b is parallel to y_p). The out-of-plane motion (indicated by θ in Fig. 2) is separately minimized by the robot's pitch control so that $\theta \approx 0$ as outlined in Section II-C below.

We let ϕ_b denote the roll angle (or rotation about y_b) of the robot, the attitude and translational dynamics of the robot and the payload are fully described by the generalized coordinates $\Phi = [\phi_b, \phi_0, \phi_1]^T$ and can be derived from the

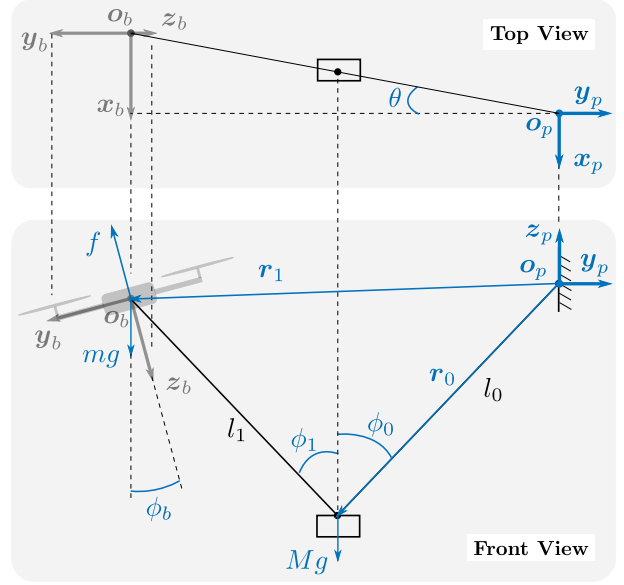


Fig. 2. (Front view) A simplified system in 2D. The payload is tethered to a follower and a fixed-point (representing a leader). (Top view) The robot and payload may deviate from the y_p - z_p plane, in which case the component of cable tension along x_p axis would provide a restoring force pulling the robot back towards the y_p - z_p plane.

Euler-Lagrange equation and corresponding the Lagrangian:

$$\tau = \frac{d}{dt} \left(\frac{\partial \mathcal{L}}{\partial \dot{\Phi}} \right) - \frac{\partial \mathcal{L}}{\partial \Phi} \quad (1)$$

$$\mathcal{L}(\Phi, \dot{\Phi}) = \mathcal{K}(\Phi, \dot{\Phi}) - \mathcal{U}(\Phi) \quad (2)$$

where

$$\mathcal{K} = \frac{1}{2} M \dot{\mathbf{r}}_0^T \dot{\mathbf{r}}_0 + \frac{1}{2} m \dot{\mathbf{r}}_1^T \dot{\mathbf{r}}_1 + \frac{1}{2} \mathbf{I}_b \dot{\phi}_b^2 \quad (3)$$

$$\mathcal{U} = [0 \quad 1] (Mg \mathbf{r}_0 + mg \mathbf{r}_1) \quad (4)$$

$$\mathbf{r}_0 = \begin{bmatrix} l_0 s(\phi_0) \\ -l_0 c(\phi_0) \end{bmatrix}, \quad \mathbf{r}_1 = \begin{bmatrix} l_0 s(\phi_0) - l_1 s(\phi_1) \\ -l_0 c(\phi_0) + l_1 c(\phi_1) \end{bmatrix} \quad (5)$$

$c(\cdot)$ and $s(\cdot)$ are shorthands for $\cos(\cdot)$ and $\sin(\cdot)$, \mathbf{I}_b is the moment of inertia about the roll axis the follower, and τ is the generalized torque evaluated according to D'Alembert's principle. Solving Eq. (1)-(5) yields the manipulator equation

$$H(\Phi) \ddot{\Phi} + C(\Phi, \dot{\Phi}) + G(\Phi) = B(\Phi) \mathbf{u} \quad (6)$$

with the following definitions:

$$H = \begin{bmatrix} 1 & 0 & 0 \\ 0 & (m+M)l_0^2 & -ml_0l_1c(\phi_0-\phi_1) \\ 0 & -ml_0l_1c(\phi_0-\phi_1) & ml_1^2 \end{bmatrix}$$

$$C = \begin{bmatrix} 0 \\ -ml_0l_1\dot{\phi}_1^2s(\phi_0-\phi_1) \\ ml_0l_1\dot{\phi}_0^2s(\phi_0-\phi_1) \end{bmatrix}, \quad G = \begin{bmatrix} 0 \\ (m+M)gl_0s(\phi_0) \\ -mgl_1s(\phi_1) \end{bmatrix}$$

$$B = \begin{bmatrix} 1 & 0 \\ 0 & l_0s(\phi_0-\phi_b) \\ 0 & l_1s(\phi_b-\phi_1) \end{bmatrix}, \quad \text{where } \mathbf{u} = \begin{bmatrix} \tau_b \\ f \end{bmatrix} \quad (7)$$

is the system's input. Finally, the nonlinear dynamics described by Eq. (6)-(7) can also be expressed using the

state vector $\mathbf{x} = [\phi_b, \dot{\phi}_b, \phi_0, \dot{\phi}_0, \phi_1, \dot{\phi}_1]^T$ as a first-order differential equation:

$$\dot{\mathbf{x}} = \mathbf{f}(\mathbf{x}, \mathbf{u}) \quad (8)$$

B. Measurement Model

Since no external feedback or additional sensors are employed, the measurements available for the follower are strictly from the onboard IMU. Since the state dynamics defined by Eq. (8) are planar, we define the output vector

$$\mathbf{y} = [\phi_b \quad \dot{\phi}_b \quad a_y \quad a_z]^T \quad (9)$$

where the angle ϕ_b and the angular rate $\dot{\phi}_b$ can be provided the complementary filter or other low level architecture, and a_y and a_z are the accelerometer readings along the y_b and z_b axes of the robot.

To obtain the measurement model, $\mathbf{y} = \mathbf{h}(\mathbf{x}, \mathbf{u})$, we first consider a minimal model of the complementary filter. Neglecting the inertial term and high-frequency dynamics, the measurement value of roll angle is approximated as the ratio of a_y to the standard gravity or $\phi_b \approx -\sin^{-1}(a_y/g)$. The gravity-subtracted acceleration, a_y and a_z , are obtained from the vector summation of the collective thrust (f) and the tension in cable l_1 (T_1), normalized by the robot's mass (m) according to $ma_y = -T_1 s(\phi_1 - \phi_b)$ and $ma_z = T_1 c(\phi_1 - \phi_b) - f$. Meanwhile, T_1 can be computed by analysing the torque dynamics of ϕ_0 about x_p , which yields

$$M l_0^2 \ddot{\phi}_0 = T_1 l_0 s(\phi_0 - \phi_1) - M g l_0 s(\phi_0) \quad (10)$$

Subsequently, the measurement model is given as

$$\mathbf{y} = \mathbf{h}(\mathbf{x}, \mathbf{u}) = \begin{bmatrix} \phi_b \\ \dot{\phi}_b \\ -(T_1/m) s(\phi_1 - \phi_b) \\ (T_1/m) c(\phi_1 - \phi_b) - (f/m) \end{bmatrix} \quad (11)$$

where T_1 is evaluated from Eq. (10), and $\ddot{\phi}_0$ from the state dynamics Eq. (8). As a result, $\mathbf{h}(\mathbf{x}, \mathbf{u})$ relates the state and input vectors to the measurement \mathbf{y} as required.

Notice that without ignoring the acceleration of the leader, it would contribute to the system's dynamics as an additional system's input. Without the knowledge of such term (via direct measurements or communication between the leader and the follower), the state would be unobservable. This illustrates the importance of the employed quasi-static assumption.

C. Out-of-plane Dynamics

Thus far, the dynamic models of the state and measurement have been derived by neglecting the out-of-plane motion or assuming the angle θ (defined about z_p) in Fig. 2 is small and the yaw angle is controlled. As a result, the position of the follower, as determined by ϕ_0 and ϕ_1 , is only dependent on the robot's roll dynamics, uncoupled from the out-of-plane motion. Here, we inspect this out-of-plane dynamics under the condition $|\theta| \ll 1$ to verify that this assumption can be satisfied in practice.

To begin, we recall that the onboard controller actively minimizes the follower's pitch angle. This means that the collective thrust lies approximately in the $\{o_p, y_p, z_p\}$ plane. As seen in Fig. 2, the motion of the robot along x_p is governed by the cable tension T_1 , that is

$$m \ddot{x}_b = -T_1 s(\phi_1) \tan \theta \quad (12)$$

Near the equilibrium state, we assume ϕ_0 , ϕ_1 and T_1 are constant. With the small angle approximation, $\tan \theta \approx \theta$ and $\ddot{x}_b \approx (-l_0 s(\phi_0) + l_1 s(\phi_1)) \ddot{\theta}$. Eq. (12) becomes

$$\ddot{\theta} = -\frac{T_1 s(\phi_1)}{m(-l_0 s(\phi_0) + l_1 s(\phi_1))} \theta \quad (13)$$

In a normal operating range, it is anticipated that $\phi_0 \in (-\frac{\pi}{2}, 0)$ and $\phi_1 \in (0, \frac{\pi}{2})$. The tension T_1 then provides a restoring torque, resulting in a marginally-stable simple harmonic oscillation. In practice, unmodeled aerodynamic damping likely produces the desirable stabilizing effect. In other words, controlling the robot's pitch and yaw angles is sufficient to ensure $\theta \rightarrow 0$, minimizing the out-of-plane motion.

III. STATE ESTIMATION & CONTROL

With the state dynamics and measurement model, in this section, we describe the estimation and control strategy to control the position of the follower robot, or realizing the ϕ_0 and ϕ_1 setpoints. To achieve this, an EKF-based estimator is proposed, allowing the state vector to be estimated from the IMU measurements. Then, a controller is derived based on a decoupled linearized state dynamics. The architecture of the estimator, controller, as well its their connections to the low-level flight controller is depicted in Fig. 3.

A. Observability and Controllability

To ensure that the state vector can be observed and controlled according to the definitions defined by Eq. (8) and (9), the dynamic model is linearized about a nominal state and verified for observability and controllability. The results show that the rank conditions of both observability and controllability matrices are satisfied.

B. State Estimation via EKF-based estimator

To estimate the state vector from available measurements, a filter or an estimator must be employed. A common solution for nonlinear dynamics and observation models is an Extended Kalman Filter, thanks to its simple implementation. However, our preliminary study reveals that EKF is unable to provide estimates with satisfactory accuracy and reliability. This is possibly due to the linearization that results in inaccurate covariance propagation. This shortcomings can be addressed by an Unscented Kalman Filter, which provides better estimation of the posterior distribution by deterministic sampling, improving the robustness and accuracy over the EKF [19]. Nevertheless, computational cost of the UKF is an order of magnitude higher than EKF [20], making the UKF unsuitable for real-time onboard implementation on a small flying robot platform without a companion computer. To this

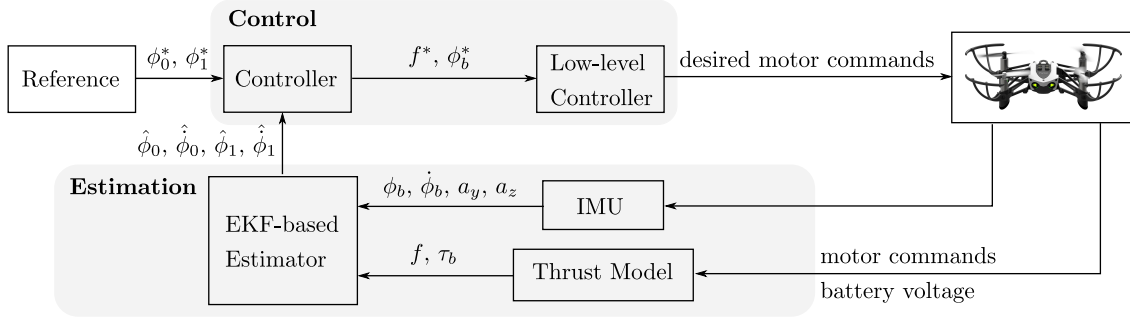


Fig. 3. The onboard estimation and control architecture. The state feedback is provided by an EKF-based estimator. The state controller computes the desired collective thrust and roll angle that can be directly used for generating motor commands by the low-level controller of the follower quadrotor.

end, we incorporated an extra tuning parameter λ into the standard EKF. Motivated by UKF, this λ plays an identical role to the parameter that controls the spread of the sigma points in UKF [19] and can be seen as a scaling parameter for adjusting the error covariance during the state prediction and update. Choosing λ to be less than unity, for instance, improves the estimator's performance when the linearization overestimates the covariance. Compared to UKF, the proposed EKF-based estimator offers rivaled performance to UKF with a similar computational requirement to EKF.

Here, we briefly describe the implementation of an EKF-based estimator. This begins by expressing the state and observation functions (Eq.(8) and (11)) in the discrete-time domain using the forward Euler method.

$$\begin{aligned} \mathbf{x}_k &= \mathbf{x}_{k-1} + \mathbf{f}(\mathbf{x}_{k-1}, \mathbf{u}_k)\Delta T + \mathbf{w}_k \\ \mathbf{y}_k &= \mathbf{h}(\mathbf{x}_k, \mathbf{u}_k) + \mathbf{v}_k \end{aligned} \quad (14)$$

where ΔT is a sample time, k denotes the time index at instant t_k , \mathbf{w}_k and \mathbf{v}_k are zero-mean Gaussian process and measurement white noises with the associated covariance matrices $\mathbf{Q}_k \in \mathbb{R}^{6 \times 6}$ and $\mathbf{R}_k \in \mathbb{R}^{4 \times 4}$. The prediction and update procedures follow closely those of standard EKF as follows.

1) *Prediction*: The prediction step resembles a standard form

$$\hat{\mathbf{x}}_k^- = \hat{\mathbf{x}}_{k-1}^+ + \mathbf{f}(\hat{\mathbf{x}}_{k-1}^+, \mathbf{u}_k)\Delta T \quad (15)$$

$$\Sigma_{\mathbf{x},k}^- = \lambda \mathbf{F}_k \Sigma_{\mathbf{x},k-1}^+ \mathbf{F}_k^T + \mathbf{Q}_k \quad (16)$$

where $\hat{\mathbf{x}}_{k-1}^+$ is an *a-posteriori* estimate at time t_{k-1} , $\hat{\mathbf{x}}_k^-$ an *a-priori* estimate at time t_k , $\Sigma_{\mathbf{x}}$ is a state covariance estimate, \mathbf{F}_k is the state Jacobian $\partial \mathbf{f} / \partial \mathbf{x} |_{\hat{\mathbf{x}}_{k-1}^+, \mathbf{u}_k}$, and λ is an extra scalar tuning parameter.

2) *Update*: The innovation covariance $\Sigma_{\mathbf{y},k}$ and Kalman gain \mathbf{K}_k are also modified to include λ as

$$\Sigma_{\mathbf{y},k} = \lambda \mathbf{H}_k \Sigma_{\mathbf{x},k}^- \mathbf{H}_k^T + \mathbf{R}_k \quad (17)$$

$$\mathbf{K}_k = \lambda \Sigma_{\mathbf{x},k}^- \mathbf{H}_k^T \Sigma_{\mathbf{y},k}^{-1} \quad (18)$$

where \mathbf{H}_k is the observation Jacobian $\partial \mathbf{h} / \partial \mathbf{x} |_{\hat{\mathbf{x}}_k^-, \mathbf{u}_k}$. Subsequently, the updated state and covariance estimates are

$$\hat{\mathbf{x}}_k^+ = \hat{\mathbf{x}}_k^- + \mathbf{K}_k (\mathbf{y}_k - \mathbf{h}(\hat{\mathbf{x}}_k^-, \mathbf{u}_k)) \quad (19)$$

$$\Sigma_{\mathbf{x},k}^+ = \Sigma_{\mathbf{x},k}^- - \lambda \mathbf{K}_k \mathbf{H}_k \Sigma_{\mathbf{x},k}^- \quad (20)$$

C. State Control

To realize cooperative transportation in the leader-follower manner by tethered flying robots, it is vital to control the cables' angles. In this part, several simplifying assumptions are employed. First, the state vector is assumed known from the estimation scheme described above. Next, the roll dynamics of the robot are presumed considerably faster than the dynamics of the tethered system. This approximation decouples the dynamics of ϕ_b from ϕ_0 and ϕ_1 , allowing the robot's thrust f and its roll angle ϕ_b to be treated as inputs of the simplified system ($\mathbf{u}_r = [f, \phi_b]^T$). The system's dynamics previously given by Eq. (6) reduce to

$$H_r(\Phi) \ddot{\Phi} + C_r(\Phi, \dot{\Phi}) + G_r(\Phi) = U_r \quad (21)$$

where H_r is constructed from the 2×2 bottom right elements of H , C_r and G_r are taken as the last two rows of C and G , and $U_r = [f l_0 s(\phi_0 - \phi_b), f l_1 s(\phi_b - \phi_1)]^T$.

For the desired constant setpoints: ϕ_0^*, ϕ_1^* , the corresponding feedforward input $\mathbf{u}_r^* = [f^*, \phi_b^*]^T$ can be found from solving the equation $G_r|_{\phi_0^*, \phi_1^*} = U_r|_{\phi_0^*, \phi_1^*, f^*, \phi_b^*}$.

To stabilize the system, Eq. (21) is linearized about the nominal conditions: $\phi_{0,1} = \phi_{0,1}^* + \Delta \phi_{0,1}$, $\mathbf{u}_r = \mathbf{u}_r^* + \Delta \mathbf{u}_r$, and $\dot{\phi}_{0,1} = 0$, this yields

$$H_r^* \Delta \ddot{\Phi} + P_r^* \Delta \dot{\Phi} = B_r^* \Delta \mathbf{u}_r \quad (22)$$

where

$$P_r^* = \frac{\partial}{\partial \Phi} (G_r - U_r) |_{\Phi^*, \mathbf{u}_r^*}, \quad B_r^* = \frac{\partial}{\partial \mathbf{u}_r} U_r |_{\Phi^*, \mathbf{u}_r^*} \quad (23)$$

It turns out that both H_r^* and P_r^* are positive definite for $-\phi_0^*, \phi_1^* \in (0, \frac{\pi}{2})$, or the linearized system is marginally stable. The structure and stability property of Eq. (21) suggests that it can be stabilized by feedback in the standard PID form

$$(H_r^{-1} B_r)^* \Delta \mathbf{u}_r = -K_p \Delta \Phi - K_d \Delta \dot{\Phi} - K_i \int \Delta \Phi dt \quad (24)$$

using the fact that H_r^* and B_r^* are always invertible as $|H_r^*| = (m^2 s^2(\phi_0^* - \phi_1^*) + mM)(l_0 l_1)^2 \neq 0$, and $|B_r^*| = f^* l_0 l_1 s(\phi_0^* - \phi_1^*) \neq 0$ at all operating points.

As a result, the follower robot is directly commanded to generate the collective thrust $f = f^* + \Delta f$, whereas the desired roll setpoint $\phi_b = \phi_b^* + \Delta \phi_b$ is given to the onboard low-level attitude controller.

It can be seen that the decision to decouple the robot's attitude dynamics from the rest of the system radically simplifies the implementation, permitting two subsystems to be separately controlled as illustrated in Fig. 3. The onboard implementation is achieved with the supplement of the EKF-based estimator and the control law described by Eq. (24), with minimal changes to the existing attitude controller.

IV. FLIGHT EXPERIMENTS AND RESULTS

To evaluate the proposed estimation and control methods, several flight experiments were conducted. First, we performed flights with a single robot, substituting the leader robot with a fixed point as assumed in the model derivation. Three sets of experiments are given to separately verify the estimation and control strategies before combining them. In the end, dual-robot experiments, in which the leader robot is present and manually controlled to follow low-speed trajectories by a human operator, are also provided.

A. Experimental Setup

Flight experiments were carried out in an indoor arena equipped with six Prime 13w motion capture (MOCAP) cameras (NaturalPoint, OptiTrack) for providing groundtruth measurements. Two Mambo Minidrones (Parrot SA) are used as the leader and follower. Each robot's mass is 73 g including markers for the MOCAP cameras. The 3D-printed dummy payload with markers weighs 30 g—a significant amount with respect to the robot's weight. It is suspended by two inelastic nylon fishing lines with 0.35 mm diameter. The cable lengths are $l_0 = 94$ cm and $l_1 = 95$ cm for all experiments. The estimation and control algorithms are implemented onboard using Simulink with the Support Package for Parrot Minidrones (MathWorks) and executed at the nominal frequency of 200 Hz. The setpoint angles were chosen as $\phi_0 = -40^\circ$ and $\phi_1 = 40^\circ$ throughout to strike the balance between efficiency (favoring small angles) and robustness (large angles preferred to avoid possible collisions). Pitch and yaw angles were directly controlled by the existing low-level attitude controller without modification. Each flight contains a total of 60 s of flying time, including 5 s for taking off and landing at the beginning and the end.

B. Implementation in 3D Space

The consideration of dynamics presented in Section II assumes that the robot's yaw angle is constant and zero. This permits us to consider the dynamics of the robot on a plane parallel to y_b and x_b axes in Fig. 2. In practice, the true yaw angle is not always zero the drift of onboard feedback, resulting in a non-zero ψ angle in the inertial frame \mathcal{W} as shown in Fig. 4. To resolve this discrepancy, frame \mathcal{P} is continuously redefined according to ψ , rendering x_p to always be parallel to x_b as previously assumed in II.

The groundtruth values of ϕ_0 and ϕ_1 are calculated from the projected plane perpendicular to x_b and x_p regardless of the actual yaw angle. Subsequently, $\dot{\phi}_0$ and $\dot{\phi}_1$ are taken as their filtered derivatives.

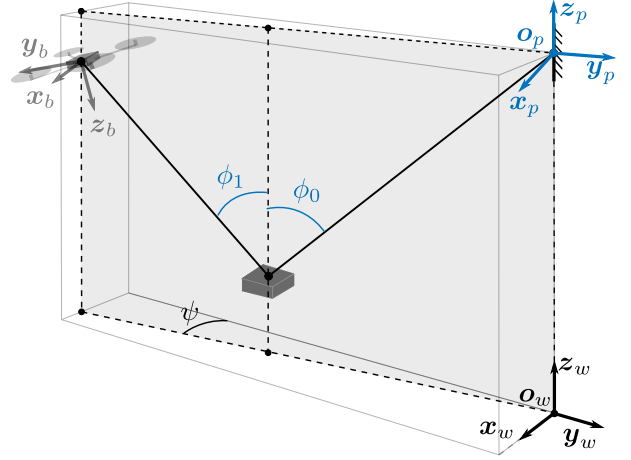


Fig. 4. Ground truth of state in 3D experimental situation. The plane y_p - z_p , in which the system is, could rotate about z_w axis due to robot's yaw motion, such that there could be an angle ψ between y_p - z_p and y_w - z_w .

C. Collective Thrust Model

Since both estimator and control strategies necessitate the knowledge of thrust as one of the system inputs, this collective force is systematically identified prior to flight experiments by mounting the robot on a loadcell (Nano25, ATI). Details of the measurement procedure are similar to the process in [2]. The collective thrust is modeled as a function of the motor commands and battery voltage (as provided by the onboard sensor of a Minidrone) using a 0th-order model. The respective model coefficients are obtained by fitting the force sensor measurements using the *n4sid* algorithm [21].

D. Single-Robot Experiments

In the first three sets of experiments, the leader robot is replaced with a fixed structure and frame \mathcal{P} becomes a true inertial frame.

1) *Open-loop flights*: To verify the estimation scheme, three open-loop flights were carried out. This means that the control law described in Section III-C only produces the feedforward input u_r^* with no corrective terms, resulting in a constant, non-zero ϕ_b^* . This is distinct from an unmodified control law, which would attempt to stabilize the robot to the roll setpoint $\phi_b^* = 0^\circ$.

These open-loop experiments are designed not only to validate the performance of the EKF-based estimator, but also to verify that, without the corrective terms in Eq. (24), the flights approximately follow the linearized dynamics in Eq. (22). This predicts a damped oscillation if unmodeled aerodynamic drag is taken into account. However, the amount of inherent aerodynamic damping is unlikely sufficient to rapidly stabilize the system.

2) *Closed-loop control with MOCAP feedback*: To evaluate the controller's performance independently from the estimation, the MOCAP was employed to compute ϕ_0 , ϕ_1 , $\dot{\phi}_0$ and $\dot{\phi}_1$ in real-time. The groundtruth feedback was wirelessly transmitted to the robot for real-time control. Three flights were performed. The state estimates were also present, but not employed for flight control.

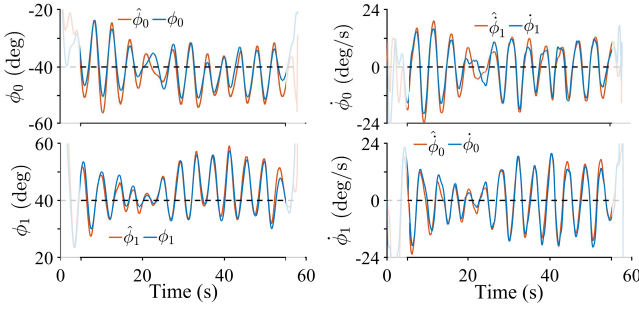


Fig. 5. Plots showing ϕ_0 , ϕ_1 and their estimates from open-loop flight.

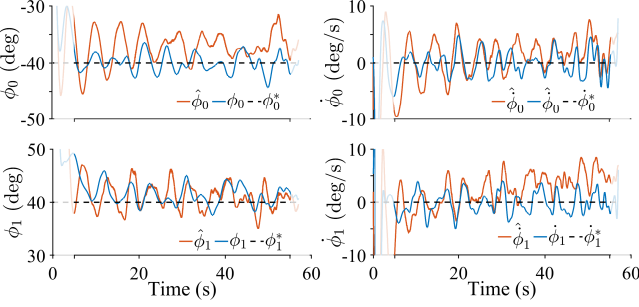


Fig. 6. Plots showing ϕ_0 , ϕ_1 and their estimates from controlled flight with MOCAP feedback.

3) *Closed-loop onboard estimation and control*: Three flights were performed with both the onboard estimation and onboard feedback for control simultaneously. In this case, the flight stability depends critically on the accuracy of the estimates.

E. Leader-Follower Experiments

Finally, to demonstrate that the proposed methods can be applied to realize cooperative transport of a suspended payload by two robots in a practical scenario where the payload is too heavy for a single robot. The fixed-point was substituted by another Parrot Mambo drone as shown in Fig. 1. We implemented a standard PID controller to the leader to control its position. The setpoint attitude of the leader was adjusted according to the nominal equilibrium condition provided by Eq. (21). This brought some slight movement to the leader's position. Three flights were performed.

F. Evaluation of Estimation and Control Methods¹

1) *Estimation results*: Fig 5 shows the estimated angles and angular rates (denoted by $\dot{\cdot}$) against the groundtruth measurements from MOCAP from one sample of the open-loop flights. It can be seen that, without the corrective control terms, both angles oscillate around the setpoints with the amplitudes of approximately $10 - 15^\circ$. The rates display a similar oscillation of up to 20 deg/s . Despite the significant and rapid variation, the estimates track the groundtruth closely, advocating the performance of the estimator. Fig. 6-8 illustrate example estimated results from the feedback controlled flights without and with the leader robot. Similar to Fig. 5, no significant estimation error is observed.

¹Example flight videos available as supplemental materials.

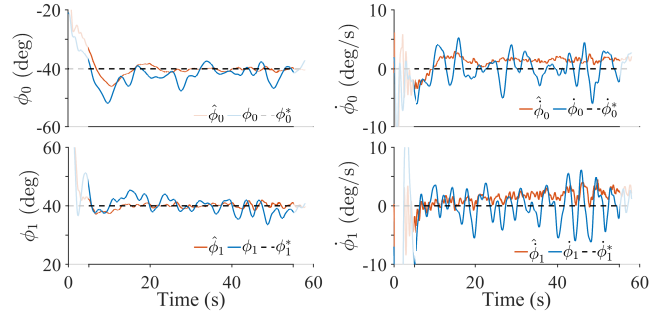


Fig. 7. Plots showing ϕ_0 , ϕ_1 and their estimates from controlled flight with onboard estimated feedback.

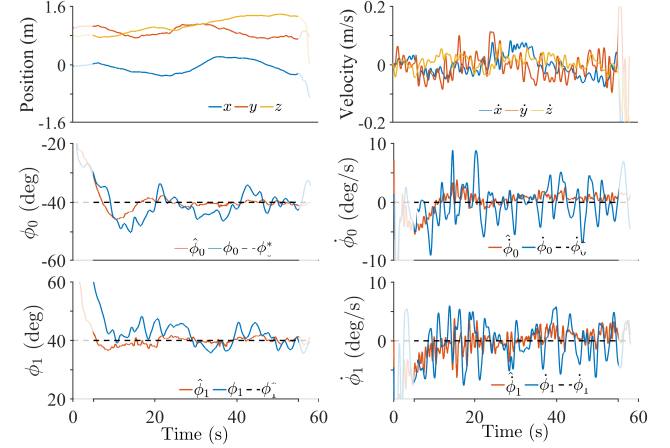


Fig. 8. Plots showing (i) position and velocity of the leader robot; and (ii) ϕ_0 , ϕ_1 and their estimates from controlled flight with onboard estimated feedback featuring two robots.

However, some slight offsets of up to 5° between $\hat{\phi}_{0,1}$ and $\phi_{0,1}$ can be seen in a few occasions. This marginal steady-state estimation error (as observed in Fig. 6) is likely caused by uncertain model parameters (such as cable's length) or the inaccuracy of thrust model. A linear sensitivity analysis around the nominal state suggests that a only 5% error in the thrust model would result in up to 15° and 20° mispredictions of ϕ_0 and ϕ_1 . With the significant change in battery levels during flight, the performance of the estimator is inevitably affected.

Quantitatively, Fig. 9(a) verifies that no significant difference between the estimation errors is visible through all 12 flights from four sets of experiments. The estimation errors are generally less than 5° or 3 deg/s . Nevertheless, errors from flights with two robots feedback tend to be higher than others, perceivably due to the violation of the assumed quasi-static conditions.

2) *Flight control performance*: To examine the performance of the flight controller, first we consider one of the open-loop flights shown in Fig. 5. Comparing groundtruths of ϕ_0 and ϕ_1 from these plots against those from closed-loop flights in Fig. 6-8, it is evident that the controller dramatically reduces the oscillation and angular errors from $> 10^\circ$ to $< 5^\circ$. Likewise, the plots of the angular rates show a substantial decrease in the angular rates from $\approx 20 \text{ deg/s}$ to $< 5 \text{ deg/s}$ when the controller is employed. The outcomes in Fig. 7 and 8 verify that small estimation errors are not detrimental

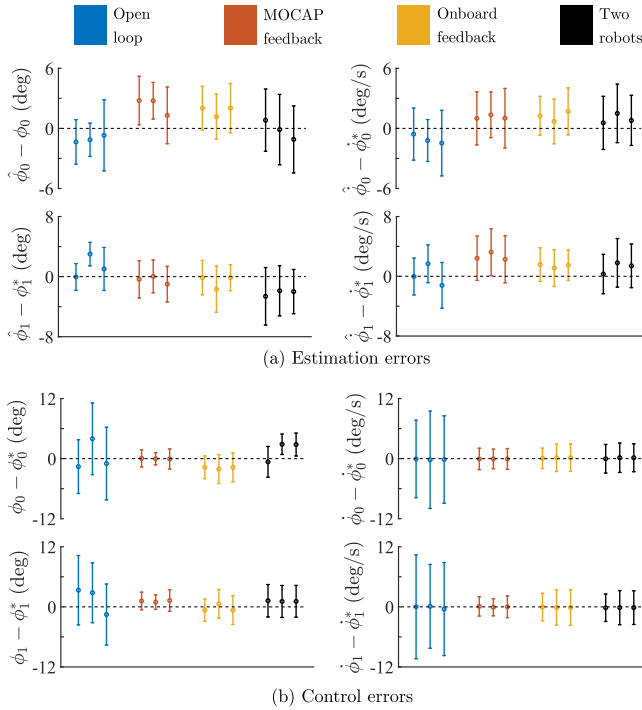


Fig. 9. (a) Means and standard deviations of the estimation errors calculated from $t = 5 - 55$ s. (b) Means and standard deviations of the control errors from $t = 20 - 55$ s to exclude the transient behavior.

to the system's stability. More comprehensive comparison between all experimental sets is provided in Fig. 9(b). As anticipated, the angular errors from flights with the MOCAP feedback are lowest—generally below a $2-3^\circ$. This is because the MOCAP feedback is not susceptible to the inaccuracy of the estimates. Furthermore, a closer inspection into the dual-robot flights there is no significant difference compared to the single-robot cases even the leader breaks the near hovering assumption as shown in the position and velocity plot in Fig. 8. Therefore, it is reasonable to conclude that the proposed strategies can be effectively applied to the scenario with two robots with low-speed maneuvers, despite the use of the fixed-point assumption in the formulation.

V. CONCLUSION AND FUTURE WORK

We presented an estimation and control strategy to address the formation control problem of two flying robots with a suspended payload. Treating the robots as a leader and a follower, the dynamics of the leader-payload-follower system is derived and the formation control problem is translated to a control of cables' angles. The proposed EKF-based estimator allows the relative position of the follower robot to be estimated using only onboard IMU measurements. With a simple feedforward PID controller, the proposed strategy has been extensively verified with flight experiments. The results demonstrate that the developed methods, which require minimal computational power, are capable of controlling the system by stabilizing the cables' angles such that they converge to the desired values with an accuracy of a few degrees.

While the strategy has been shown feasible in practice, it is not without limitations. Thus far, the methods rely on two

major simplifying assumptions, the neglect of the inertial effect of the leader and the planar consideration. Future work will take into account the acceleration of the leader to eliminate the quasi-static assumption and then extend the work to account for non-planar dynamics.

REFERENCES

- [1] Y. Chen, H. Zhao, J. Mao, P. Chirattananon, E. F. Helbling, N.-s. P. Hyun, D. R. Clarke, and R. J. Wood, "Controlled flight of a microrobot powered by soft artificial muscles," *Nature*, vol. 575, no. 7782, pp. 324–329, 2019.
- [2] Y. H. Hsiao and P. Chirattananon, "Ceiling effects for hybrid aerial-surface locomotion of small rotorcraft," *IEEE/ASME Transactions on Mechatronics*, 2019.
- [3] Y. Mulgaonkar, A. Makineni, L. Guerrero-Bonilla, and V. Kumar, "Robust aerial robot swarms without collision avoidance," *IEEE Robotics and Automation Letters*, vol. 3, no. 1, pp. 596–603, 2017.
- [4] M. A. Estrada, S. Mintchev, D. L. Christensen, M. R. Cutkosky, and D. Floreano, "Forceful manipulation with micro air vehicles," *Science Robotics*, vol. 3, no. 23, p. eaau6903, 2018.
- [5] B. Mu and P. Chirattananon, "Universal flying objects: Modular multirotor system for flight of rigid objects," *IEEE Transactions on Robotics*, 2019.
- [6] G. Loianno and V. Kumar, "Cooperative transportation using small quadrotors using monocular vision and inertial sensing," *IEEE Robotics and Automation Letters*, vol. 3, no. 2, pp. 680–687, 2017.
- [7] D. G. Morin, J. Araujo, S. Tayamon, and L. A. Andersson, "Autonomous cooperative flight of rigidly attached quadcopters," in *2019 International Conference on Robotics and Automation (ICRA)*. IEEE, 2019, pp. 5309–5315.
- [8] A. Tagliabue, M. Kamel, R. Siegwart, and J. Nieto, "Robust collaborative object transportation using multiple mavs," *The International Journal of Robotics Research*, vol. 38, no. 9, pp. 1020–1044, 2019.
- [9] K. Sreenath and V. Kumar, "Dynamics, control and planning for cooperative manipulation of payloads suspended by cables from multiple quadrotor robots," in *Proc. Conf. Robotics: Science and Systems*, 2013.
- [10] M. Gassner, T. Cieslewski, and D. Scaramuzza, "Dynamic collaboration without communication: Vision-based cable-suspended load transport with two quadrotors," in *2017 IEEE International Conference on Robotics and Automation (ICRA)*. IEEE, 2017, pp. 5196–5202.
- [11] R. M. Murray, "Trajectory generation for a towed cable system using differential flatness," in *IFAC world congress*, 1996, pp. 395–400.
- [12] K. Sreenath, N. Michael, and V. Kumar, "Trajectory generation and control of a quadrotor with a cable-suspended load—a differentially-flat hybrid system," in *2013 IEEE International Conference on Robotics and Automation*. IEEE, 2013, pp. 4888–4895.
- [13] S. Tang and V. Kumar, "Mixed integer quadratic program trajectory generation for a quadrotor with a cable-suspended payload," in *2015 IEEE International Conference on Robotics and Automation (ICRA)*. IEEE, 2015, pp. 2216–2222.
- [14] G. Yu, D. Cabecinhas, R. Cunha, and C. J. Silvestre, "Nonlinear backstepping control of a quadrotor slung load system," *IEEE/ASME Transactions on Mechatronics*, 2019.
- [15] E. L. de Angelis, F. Giulietti, and G. Pipeleers, "Two-time-scale control of a multirotor aircraft for suspended load transportation," *Aerospace Science and Technology*, vol. 84, pp. 193–203, 2019.
- [16] N. Michael, J. Fink, and V. Kumar, "Cooperative manipulation and transportation with aerial robots," *Autonomous Robots*, vol. 30, no. 1, pp. 73–86, 2011.
- [17] T. Lee, "Geometric control of quadrotor uavs transporting a cable-suspended rigid body," *IEEE Transactions on Control Systems Technology*, vol. 26, no. 1, pp. 255–264, 2017.
- [18] B. Shirani, M. Najafi, and I. Izadi, "Cooperative load transportation using multiple uavs," *Aerospace Science and Technology*, vol. 84, pp. 158–169, 2019.
- [19] F. Gustafsson and G. Hendeby, "Some relations between extended and unscented kalman filters," *IEEE Transactions on Signal Processing*, vol. 60, no. 2, pp. 545–555, 2011.
- [20] D. Simon, "A comparison of filtering approaches for aircraft engine health estimation," *Aerospace Science and Technology*, vol. 12, no. 4, pp. 276–284, 2008.
- [21] W. Favoreel, B. De Moor, and P. Van Overschee, "Subspace state space system identification for industrial processes," *Journal of process control*, vol. 10, no. 2-3, pp. 149–155, 2000.